


*17th World Conference on Earthquake Engineering, 17WCEE*
*Sendai, Japan - September 13th to 18th 2020*

# EXPERIMENTAL AND NUMERICAL STUDY OF SPHERICAL SLIDING BEARING (SSB) PART 2: FRICTION MODELS

Jiaxi Li[(1)], Satoshi Yamada[(2)], Shoichi Kishiki[(3)], S. Yamazaki[(4)], A. Watanabe[(5)], M. Terashima[(6)]

[(1)] *Graduate student, Tokyo institute of technology, li.j.ax@m.titech.ac.jp*
[(2)] *Professor, Tokyo institute of technology, Dr. Eng. yamada.s.ad@m.titech.ac.jp*
[(3)] *Associate Prof., Tokyo Institute of Technology, Dr. Eng. kishiki.s.aa@m.titech.ac.jp*
[(4)] *Senior manager, Dr. Eng, Nippon Steel Engineering Co., Ltd. yamazaki.shinsuke.f5g@eng.nipponsteel.com*
[(5)] *Senior manager, Nippon Steel Engineering Co., Ltd. watanabe.atsushi.8hx@eng.nipponsteel.com*
[(6)] *Manager, Ph.D., Nippon Steel Engineering Co., Ltd. terashima.masao.mx4@eng.nipponsteel.com*

## *Abstract*

Friction pendulum bearings (FPBs), which are a type of base isolation technique that detaches structures from the ground to help stabilize buildings from earthquakes, are widely used in earthquake-prone regions and SSB is a type of double concave friction pendulum bearing (DCFPB) developed in Japan. Many methods for obtaining dependency Equations or simulating temperature caused by friction heating and friction models that combine dependency Equations together were proposed, but few of these friction models were comprehensively validated with a sufficient number of experiments containing various loading conditions. Most of the models were checked under only one or two types of seismic load. In this article, the analysis results of three friction models are compared with experimental results under various loading conditions, for which the aim is to research whether the error of each model is acceptable under these conditions, i.e., the applicability of each model.

Therefore, the purpose of this study is to propose comprehensively validated friction models and evaluate their applicability. To achieve this aim, 22 full-scale unidirectional dynamic tests results on 2 sizes of specimens are used to validate the pressure and velocity dependency Equations proposed in a previous study. The temperature dependency Eq. proposed in a previous study and the temperature simulation method proposed by MC. Constantinou et al. are also introduced. Based on these, three friction models (precise, simplified and constant models) were proposed. In addition, the test results of 48 different full-scale unidirectional dynamic tests, which are considered to contain various conditions that a DCFPB may experience during service based on an ASCE standard, were quoted from a previous study; these tests included various parameters, such as different pressures, velocities, excitation amplitudes, numbers of cycles and slider diameters. The three friction models were validated through a comparison with the experimental data obtained from these tests. The accuracy of both the hysteresis curves and the force-deflection characteristics were checked under various parameters, and the applicability of the three models was discussed. (1) The precise model, which considers the influence of pressure, velocity and temperature (by over 150 monitor points) on the friction coefficient, has high accuracy except when the friction heating is extremely high. (2) The simplified model, whose main difference from the precise model is that it has only one monitor point for simulating the temperature, has high accuracy under most situations except those with oscillation amplitudes larger than the slider diameter. (3) The constant model uses a constant friction coefficient, and the difference in accuracy between this model and the other models is not significant.

*Keywords: Double concave friction pendulum bearing; Friction models; Friction dependencies*

## 1. Introduction

Friction pendulum bearings (FPBs), which are a type of base isolation technique that detaches structures from the ground to help stabilize buildings from earthquakes, are widely used in earthquake-prone regions. This article focuses on double concave FCBs (DCFPBs) as shown in Fig. 1.

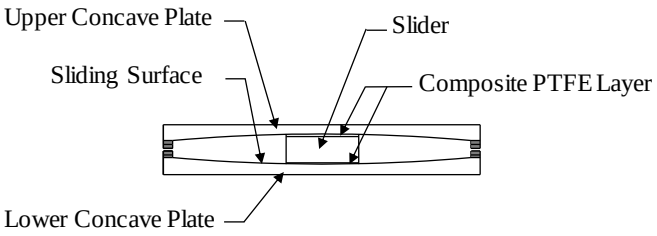


Fig. 1 – Composition of a DCFPB

The clear force-displacement relationship of FPBs makes numerical analysis one of the best ways to study and predict the performance of them, wherein the mainly focus is on the calculation of Friction force ($F_f$). This focus on $F_f$ is because the dependency of the friction coefficient on pressure, velocity and temperature is the most important characteristic for the performance of an FPB. Therefore, the lubricant material used in an FPB and the characteristics of this material are very important. Quaglini et al. (2012) proposed an experimental methodology for the characterization of self-lubricating materials based on pressure, velocity, external temperature and displacement through small-scale specimens [1]. In addition to the external temperature, particular attention was paid to the temperature increase at the sliding surface caused by friction heating because this increase in temperature had a significant influence on the behavior of an FPB during an earthquake event, which is a kind of strong or long duration seismic excitation. Moreover, the measurement of this temperature increase is very difficult during dynamic excitation. In this respect, Lomiento et al. (2013) proposed a friction model that takes into account the vertical load, velocity and cycling effect (degradation of friction characteristics due to repetition of cycles and consequent temperature rise) by performing 1D prototype dynamic tests on single concave FPBs (SCFPBs) [2]. Quaglini et al. (2014) proposed a 3D finite element model (FEM) of an SCFPB to estimate friction heating, and the estimated temperature was validated with experimental data measured by thermocouples embedded in the concave sliding plate [3]. Following this work, some studies proposed simplified temperature simulation methods. Kumar et al. (2015) proposed a simplified model to calculate the representative temperature of the sliding surface for thermal calculations (method 2 in the article) considering the pressure, velocity and temperature dependency, and the analysis results were verified by 2D prototype dynamic tests of SCFPBs [4]. The distributions of maximum displacement under 30 sets of ground motions (GMs) in the original model (method 1 in the article) and the simplified model were compared, and a relatively small difference was found between the models; thus, the simplified model could be applied instead of the original model. Then, with the appearance of multiple concave FPBs (MCFPBs), Bianco et al. (2018) proposed a simplified rheological model to simulate the temperature rise in MCFPBs [5].

Most of these studies proposed new methods for obtaining dependency Equations or simulating temperature caused by friction heating and new friction models that combine dependency Equations together, but few of these friction models were comprehensively validated with a sufficient number of experiments containing various loading conditions. Most of the models were checked under only one or two types of seismic load. Although the pressure, velocity and temperature dependency Equations were individually determined under their possible range, it is still necessary to validate the accuracy of the friction model under a sufficient number of loading conditions because of the interaction among the dependencies. Only when these conditions are met can the applicability of the friction models be determined. The applicability of the friction model is important because assumptions are usually made for numerical models, which will make it difficult to obtain accurate analysis results from the models under all situations. In this article, the analysis



 

results of three models are compared with experimental results under various loading conditions, for which the aim is to research whether the error of each model is acceptable under these conditions, i.e., the applicability of each model.

## 2. Friction model

Pressure, velocity and temperature dependency equations from previous studies [8~10] are introduced in this section, and the applicability of the pressure and velocity dependency Equations for φ300 and φ400 specimens are verified by the dependency test introduced in part 1. Since the temperature is difficult to accurately measure during testing, a numerical method proposed by MC. Constantinou et al. [11, 4] was also introduced to simulate the temperature. Based on these Equations, three friction models are described: precise, simplified and constant models.

### 2.1 Pressure, velocity and temperature dependency of the friction coefficient

The pressure dependency of the friction coefficient can be considered by a pressure dependency factor $\gamma$, which is related to the bearing stress $\sigma$ at the contact area of the concave plate and slider. The pressure dependency equation is obtained by a previous experimental study [8]:

$$\gamma = 2.03 \times \sigma^{-0.19} + 0.068 \tag{1}$$

Also, the dependency of the friction coefficient on velocity is considered by a velocity dependency factor $\alpha$. This factor is related to the velocity of the upper concave plate relative to the lower concave plate $v$, which can be described by the following equation [8]:

$$\alpha = 1 - 0.55 \times e^{-0.019v} \tag{2}$$

Fig. 2 shows the applicability verification of the pressure and velocity dependency Equations for φ300 and φ400 specimens based on the dependency test introduced in part 1. In Fig. 2, the experimental friction coefficients calculated from the dependency test are normalized by the values at 60 N/mm2 and 400 mm/s, respectively, to minimize the influence of product variation. As a result, Equations (1) and (2) both show high consistency with the experimental results, so the previously proposed pressure and velocity dependency equations are also effective for DCFPBs with φ300 and φ400 slider diameters.

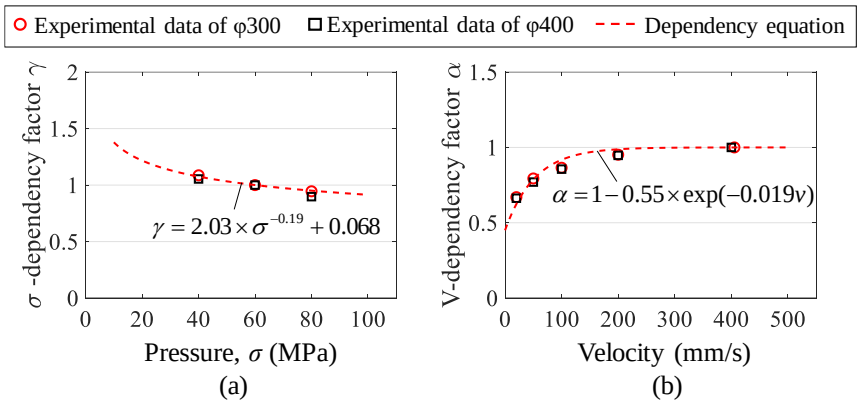


Fig. 2 – Verification of (a) pressure and (b) velocity dependency Equations by dependency test

The temperature dependency Eq. is shown as follows:

$$\beta = 1.13 \times \exp(-0.007T) \tag{3}$$

where $\beta$ is the temperature dependency factor and $T$ is the temperature of the contact area between the slider and the concave plate in Celsius [9, 10].



 

## 2.2 Temperature computation of friction heating

A general computation of temperature at the surface of a semi-infinite solid with heat flux q(t) that varies with time is shown as follows [4, 11]:

$$\Delta T(t) = \frac{\sqrt{D}}{k\sqrt{\pi}} \int_0^t \frac{q(t-\tau)d\tau}{\sqrt{\tau}} \tag{4}$$

where $q(t)$ is the heat flux at the surface of the solid, $\Delta T(t)$ is the temperature increase at time $t$ compared with the temperature at $t$=0, $\tau$ is a time parameter that varies between 0 and $t$, $D$ is the thermal diffusivity of the solid, and $k$ is the thermal conductivity of the solid [11]. In this study, the values of $k$ and $D$ are adopted from the "JSME Data Book: Heat Transfer", which are 0.016 W/(mm·°C) and 4.07 mm2/s, respectively [12].

For DCFPBs, the instantaneous heat flux, $q(t)$, can be defined as follows:

$$q(t) = \begin{cases} \mu(t)p(t)\dfrac{v(t)}{2} & \text{if } \delta \le \sqrt{\pi \cdot r_{contact}{}^2}/2 \\ 0 & \text{otherwise} \end{cases} \tag{5}$$

where $\mu(t)$, $p(t)$ and $v(t)$ are the coefficient of friction, the pressure at the contact area and the relative velocity between the upper and lower concave plates at time $t$, respectively; $\delta$ is the lateral distance from the center of the slider to the point of interest; and $r_{contact}$ is the contact radius [4].

## 2.3 Representative temperature of the sliding surface

Fig. 3 shows the calculation method for the representative temperature. The small circles in Fig. 3 are the analytical monitor points. These monitoring points are virtual points set up in the friction model, whose temperature can be calculated by eq. (4) and (5) at any time during excitation.

Fig. 3 (a) shows the monitor point distribution for the precise model (the number of monitor points shown in the figure is much less than that used in the model). The temperature is tracked on a line of uniformly distributed points along the sliding direction across the center of the slider on the sliding surface with an interval of 5 mm. The average value of the temperatures at the points within the contact area is used for T in Eq. (3). Here, the section of the slider is assumed as a square with an area equal to the area of the slider (contact area). Because the contact area is assumed to be a square, one line of monitor points in the direction of sliding shown in Fig. 3 (a) can give the same result as a grid of monitor points.

Fig. 3 (b) shows a simplified method proposed by M. Kumar et al., in which only the temperature at the center of the sliding surface is used to compute T in Eq. (3) [4]. In this case, when the slider is above the center point, T in Eq. (3) will increase, and when the slider moves away, the temperature will decrease.

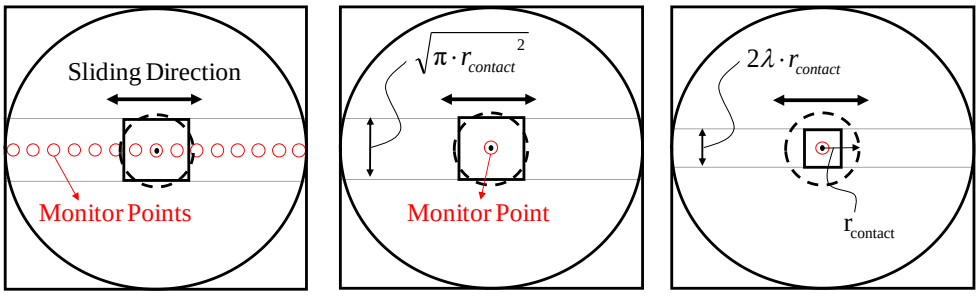


(a) (b) (c)

Fig. 3 – Calculation method for representative temperature for the (a) precise model (monitor points placed at an interval of 5 mm), (b) simplified model (1 monitor point at the center) and (c) refined simplified model



 

However, the temperature calculated by the simplified model is always higher than that calculated by the precise model, as shown in Fig. 4, which shows the temperature history of the precise model and simplified model under ASCE test φ300 T12a introduced in part 1. This discrepancy exists because, under unidirectional sinusoidal displacement variation, the monitor point at the center of the concave plate always has the highest heat flux input; hence, this point will have the highest temperature throughout the majority of the test, and the other monitor points have lower temperatures. Therefore, as the simplified model has only one monitor point at the center, this model will tend to overestimate the temperature.

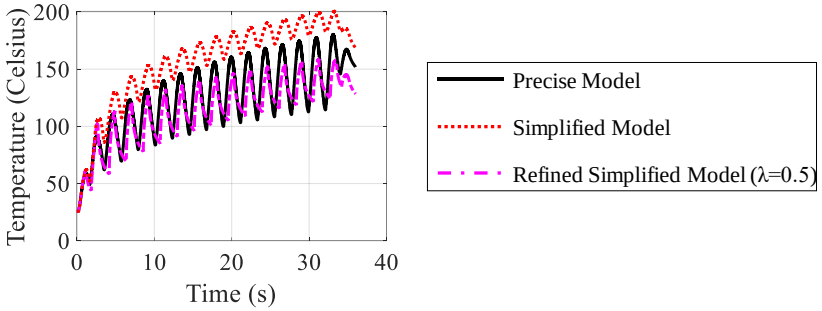


Fig. 4 – Temperature history (simulated temperature of the contact area between the slider and the concave plate) comparison of the precise model, simplified model and refined simplified model

Thus, in this study, a refinement factor $\lambda$ = 0.5 on $r_{contact}$ is proposed to consider this influence for the simplified method, as shown in Fig. 3 (c), and the temperature history of the refined simplified model shows better fitness with the precise model than the simplified model, as shown in Fig. 4. Therefore, for the refined simplified model, the instantaneous heat flux, q(t), will be calculated by eq. (6) and the phrase 'simplified model' in the following tests will represent the refined simplified model.

$$q(t)=\begin{cases}\mu(t)p(t)\dfrac{v(t)}{2} & \text{if } \delta \le \lambda \cdot r_{contact} \\ 0 & \text{otherwise}\end{cases} \tag{6}$$

## 2.4 Friction model that combines pressure, velocity and temperature dependencies

The friction coefficient of the precise and simplified model at each time during excitation is calculated by:

$$\mu_t = \mu_{to} \times \gamma \times \alpha \times \beta \tag{7}$$

where $\mu_t$, $\gamma$, $\alpha$, and $\beta$ are the friction coefficient, pressure dependency factor, velocity dependency factor and temperature dependency factor, respectively, and $\mu_{to}$ is the friction coefficient at 60 N/mm$^2$ ($\gamma$ =1), 400 mm/s ($\alpha$=1) and 20˚C ($\beta$ =1), which is selected as 0.075 for all specimens. This is a pseudo friction coefficient calculated by the trend line of friction coefficient versus time in dependency test-φ300-T05 (introduced in part 1) when time approaching zero, as shown in Fig. 5. The experimental value is the friction coefficient near zero displacement where the velocity is 400 mm/s and the pressure is 60 N/mm$^2$.

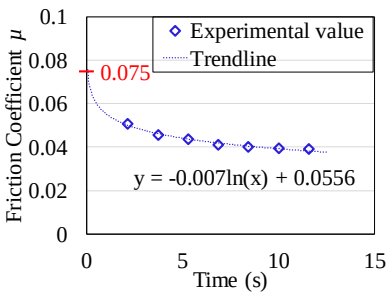


Fig. 5 – Determination of $\mu_{to}$



 

A constant model is also proposed. The idea of this model is to find a constant friction coefficient that is suitable for the most time during most situations. This constant value is calculated as follows:

$$\mu_c = \mu_0 \times \gamma(\sigma_d) \times \alpha(v_d) \times \beta(T_0) \quad (8)$$

where $\mu_0$ is the reference friction coefficient, $\gamma(\sigma_d)$ is the pressure dependency factor at the designed pressure of the test, $\alpha(v_d)$ is the velocity dependency factor at the designed maximum velocity of the test and $\beta(T_0)$ is the temperature dependency at the initial temperature of the test. Note that $\mu_0$ is 0.041 for a DCFPB with a 300 mm slider diameter and 0.038 for a DCFPB with a 400 mm slider diameter based on experimental results, representing the reference friction coefficient under average load conditions: 400 mm/s and 60 N/mm2. These values are determined by taking the average of the friction coefficient of a DCFPB at zero displacement points in the second cycle (points c and d in fig. 6) of the sine wave with a constant pressure 60 N/mm2 and a maximum velocity of 400 mm/s (T05 of dependency test in table 2 of part 1).

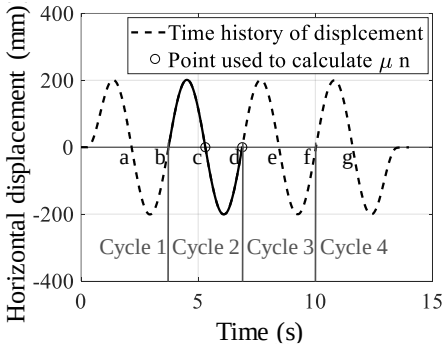


Fig. 6 – Experimental data used to obtain the reference friction coefficient

## 3. Validation and applicability of the friction models

This section validates the accuracy of the hysteresis curves and force-deflection characteristics of the three models and discusses the applicable range of each model.

### 3.1 Force-deflection characteristics

For unidirectional tests with sinusoidal displacement excitation, the force-deflection characteristics are the most important characteristics that show the behavior of a bearing. In this section, the accuracy of the $F_{max}$ (maximum horizontal force), $F_{min}$ (minimum horizontal force), $K_{ru}$ (upper post yield stiffness), $K_{rl}$ (lower post yield stiffness), $EDC$ (energy dissipated per cycle), $K_{eff}$ (effective stiffness) and $\beta_{eff}$ (effective damping) calculated by the three models are evaluated. Fig. 7 and eq. (9) ~ (11) show the method used to calculate these values [7]. The values of $K_{ru}$ and $K_{rl}$ are calculated by the least-squares method, and $EDC$ is calculated by an integral.

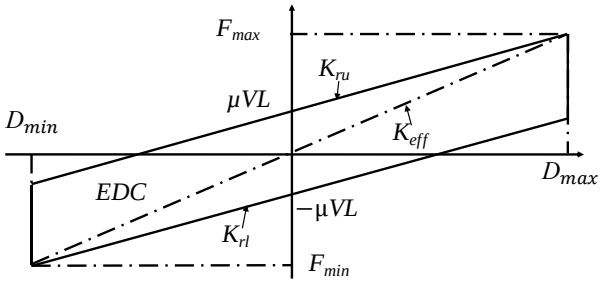


Fig. 7 – Force-deflection characteristics of a DCFPB bilinear model



 

$$K_{ra} = \frac{|K_{ru}| + |K_{rl}|}{2} \tag{9}$$

$$K_{eff} = \frac{|F_{\max}| + |F_{\min}|}{|D_{\max}| + |D_{\min}|} \tag{10}$$

$$\beta_{eff} = \frac{2}{\pi} \frac{EDC}{K_{eff}\,(|D_{\max}| + |D_{\min}|)^2} \tag{11}$$

### 3.2 Effect of accumulated displacement on the behavior of the bearing

The effect of accumulated displacement is checked by comparing the 1st cycle of the two production tests at the beginning and the ending (T01 and T13 of) of the ASCE test - φ300 and 400 (introduced in part 1), as shown in fig. 8. The accumulated displacements of the 1st cycle of T01 and T13 are approximately 0 and 67 meters, respectively. The figure shows that the effect can be neglected, so in the later discussion, the effect of accumulated displacement will not be considered.

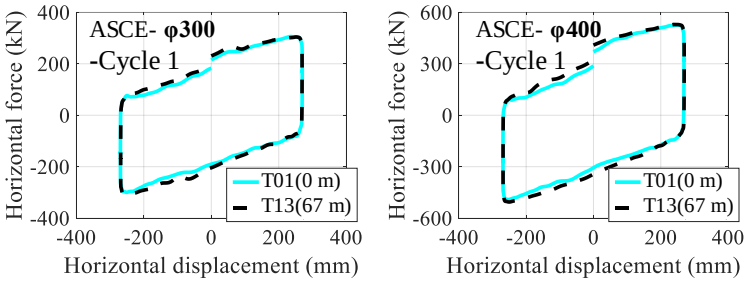


(a) (b)

Fig. 8 – Effect of accumulated displacement on the (a) φ300 specimens and (b) φ400 specimens

### 3.3 Validation under different numbers of cycles

The influence of long duration excitation on a DCFPB is considered by ASCE test T12 with a large number of cycles. Usually, during an earthquake, the orbit of the bearing is rarely repeated in the same route, so the seismic loading conditions (tests in the ASCE tests except T02) when the number of cycles is greater than 3 (cycle 4, cycle 5…) can be considered as "extremely high friction heating conditions". Additionally, to avoid the effect of friction heating, the 1st cycle of the hysteresis curve will be used to validate the accuracy of the friction models on the other factors in later discussions.

Fig. 9 shows the fitness of the hysteresis curves of the precise and constant models under cycles 1, 4 and 7 through a comparison with the experimental results of the ASCE test φ300-T12a. For the precise model, the decrease in the absolute value of the maximum forces caused by friction heating fits well with the experimental result as the number of cycles increases. However, in cycle 4 and 7 (extremely high friction heating conditions), the horizontal force near zero displacement of the precise model is slightly lower than that of the experimental result. This discrepancy exists because the temperature here was overestimated.

To see the effect clearly, the values of *EDC*, $K_{eff}$ and $\beta_{eff}$ are calculated and compared with the experimental result of φ300-T12a for all cycles, as shown in fig. 10. Because of the refinement factor $\lambda$, the simplified model has the best result, for which the error of all characteristics is within 10%. The precise model is accurate for $K_{eff}$ within 10% error because of the good fitness of maximum forces, but this model has lower accuracy for $\beta_{eff}$, which has a maximum error within 20% at cycle 7. The constant model shows low accuracy for both *EDC* and $K_{eff}$ at a large number of cycles because the increasing temperature caused by friction heating is not considered over time. In conclusion, the precise model and constant model show low accuracy when the friction heating is extremely high.



 

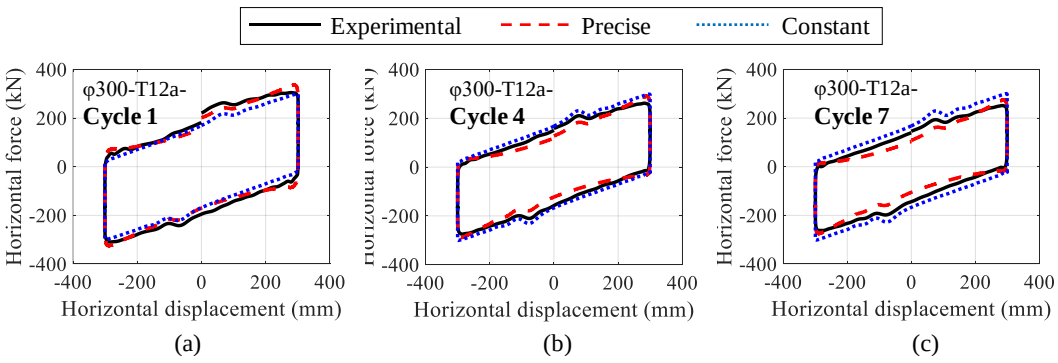


Fig. 9 – Comparison of hysteresis curves under different cycles (ASCE φ300-T12a)

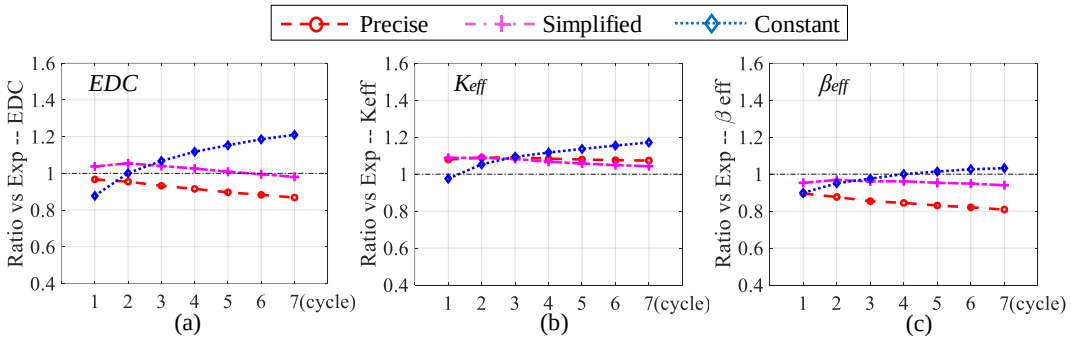


Fig. 10 – Comparison of force-deflection characteristics under different cycles (ASCE φ300-T12a)

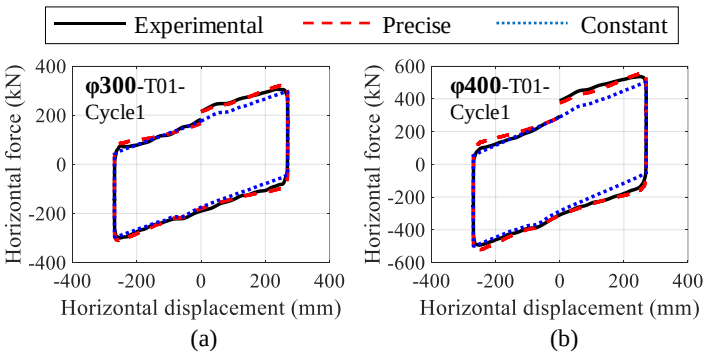


Fig. 11 – Comparison of hysteresis curves under different slider diameters (ASCE tests)

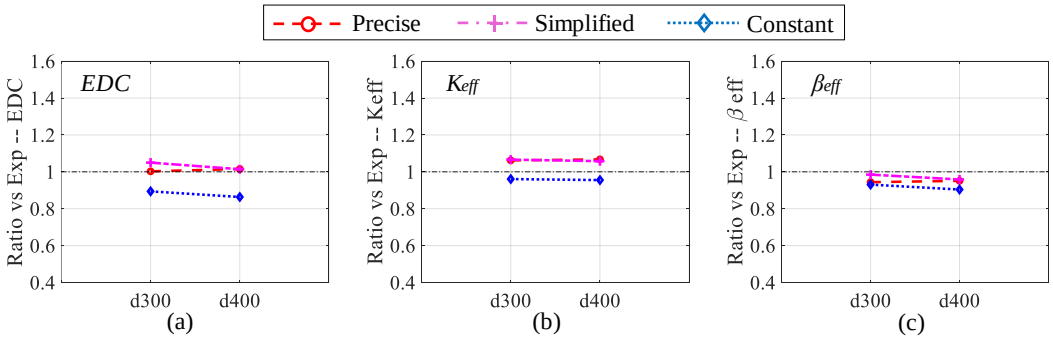


Fig. 12 – Comparison of force-deflection characteristics under different slider diameters (based on ASCE tests φ300-T01 and φ400-T01-cycle 1)



 

### 3.4 Validation under different slider diameters

Fig. 11 and fig. 12 show good fitness for all three models under different slider diameters. This finding means that the three models are basically applicable under different slider diameters.

### 3.5 Validation under different velocities and oscillation amplitudes

In the ASCE tests, the loading period is constant (4.26 s) for every test, and the maximum velocity is calculated from the oscillation amplitude; thus, in this part, the model accuracies under different velocities and oscillation amplitudes are validated together.

Fig. 13 shows the fitness of three friction models with the experimental results. Fig. 13 (a), (b) and (c) shows that the precise model has high accuracy under various velocities ranging from 146 mm/s to 585 mm/s. The constant model shows low accuracy at low velocity, 146 mm/s; however, the error of $K_{eff}$ at 146 mm/s reduces to 5% at cycle 3. For the simplified model, figure 13 (d), (e) and (f) shows that for a DCFPB with a φ300 slider, a force jump will occur when the displacement equals 150 mm, which is half of the slider diameter, and the influence of this force jump will be larger when the oscillation amplitude is larger.

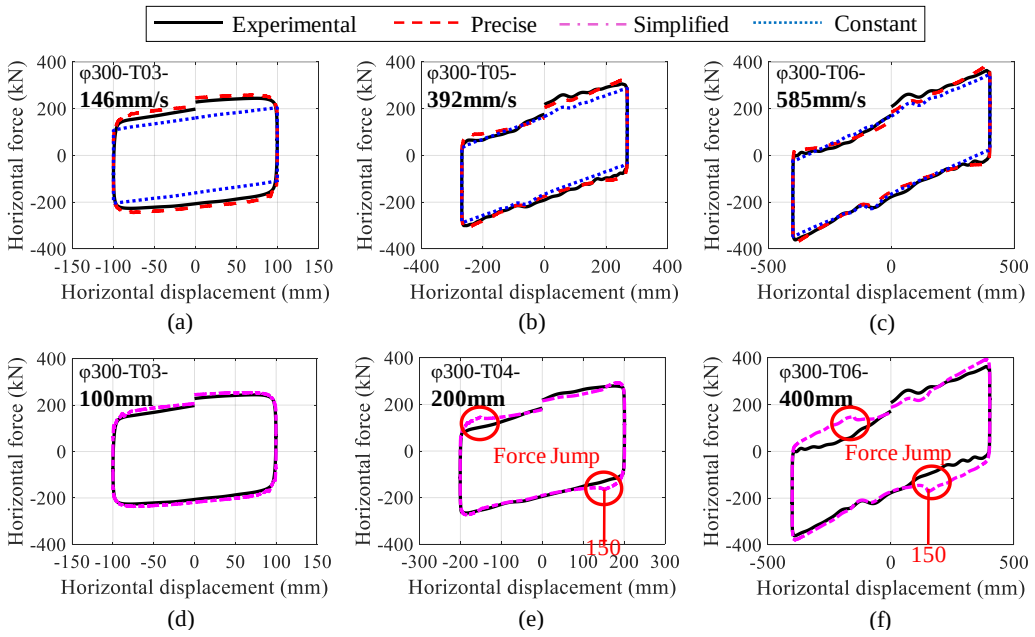


Fig. 13 – Comparison of hysteresis curves under different velocities and oscillation amplitudes (ASCE test-cycle 1)

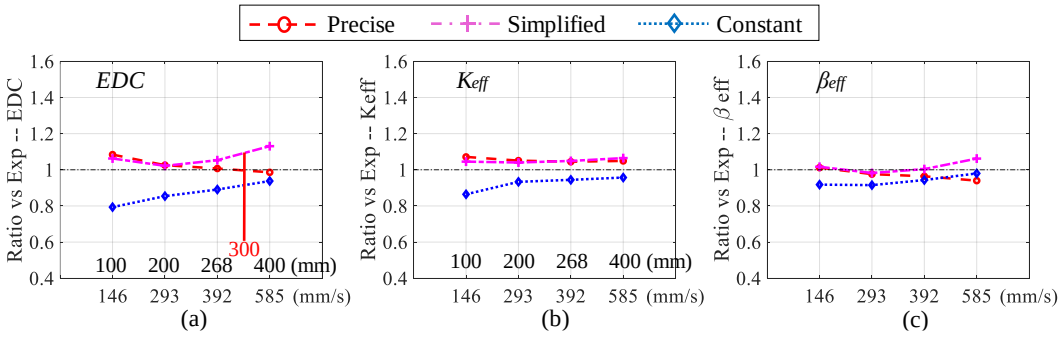


Fig. 14 – Comparison of force-deflection characteristics under different velocities and oscillation amplitudes (based on ASCE test-φ300-T03, T04, T05, T06-cycle 1)



 

Fig. 14 clearly shows the effect of different velocities and oscillation amplitudes. When the oscillation amplitude is larger than 300 mm, which is the diameter of the slider, the error of *EDC* calculated from the simplified model will exceed 10%. This finding means that the simplified model has low accuracy when the oscillation amplitude is larger than the diameter of the slider.

### 3.6 Validation under different pressure

Fig. 15 and 16 show that the precise model still has high accuracy. The performance of the simplified model is not good because of the high velocity (large oscillation amplitude) of the tests, but fig. 16 shows that the influence of pressure is small because the slope is small, which means that the simplified model is suitable under different velocities. Similar to the situation under low velocity, the constant model shows lower accuracy under low pressure at cycle 1 because of low friction heating.

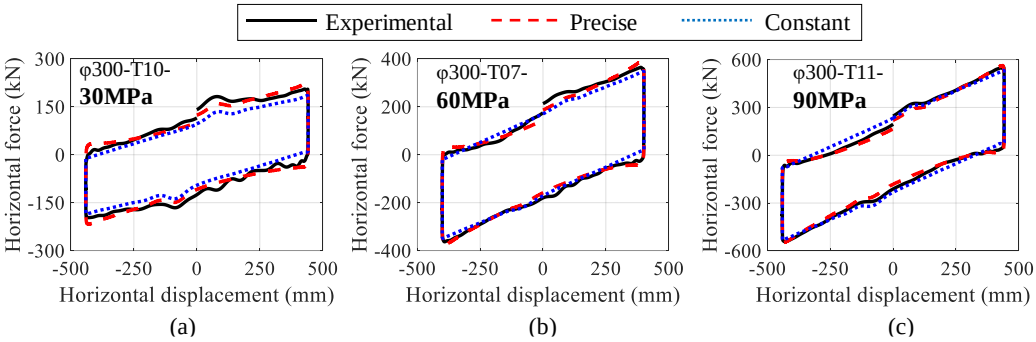


Fig. 15 – Comparison of hysteresis curves under different pressures (cycle 1)

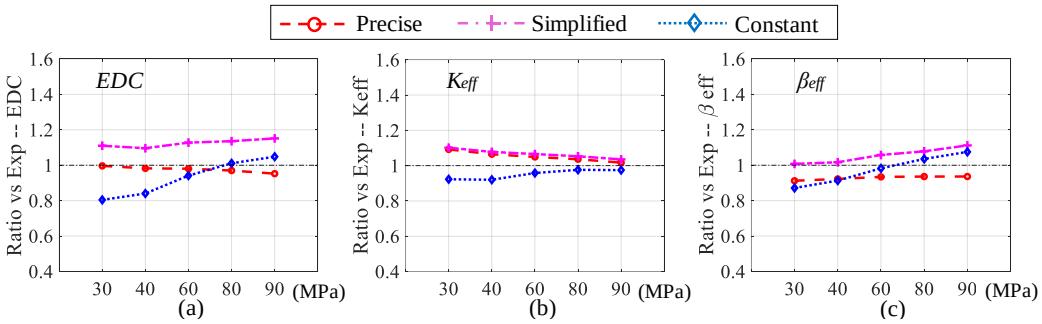


Fig. 16– Comparison of force-deflection characteristics under different pressures (based on ASCE test-φ300-T10, T08, T07, T09, T11-cycle 1)

### 3.7 Validation under small velocities and small loads

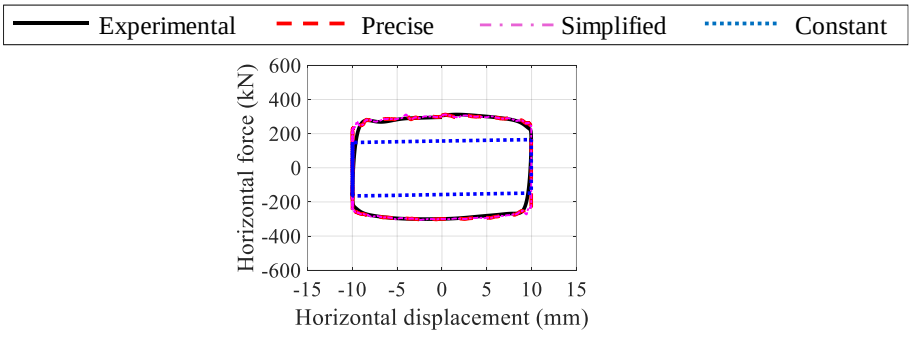


Fig. 17 – Comparison of hysteresis curves under small loads (ASCE test-φ400- T02-cycle 1)



 

Fig. 17 shows the validation of the hysteresis curves of the three friction models under loads with extremely small velocities, wherein the maximum velocity is approximately 15 mm/s, simulating a wind load. The precise model and simplified model both have high accuracy. However, the horizontal force simulated by the constant model is much smaller than the experimental result because when the reference friction coefficient considered in the constant model is determined, it already includes a certain decrease in friction coefficient caused by friction heating, which is common for earthquake excitations. However, for a wind load, the friction coefficient decrease caused by friction heating is much smaller than that in an earthquake, so the horizontal force simulated by the constant model is smaller than the experimental result.

## 4. Summary and conclusions

Three friction models were introduced and validated with full-scale unidirectional dynamic tests under various loading conditions, and the applicability of these three models was evaluated.

The precise model shows higher applicability than the other two models, including various pressures, velocities, oscillation amplitudes, numbers of cycles and slider diameters. However, the precise model overestimates the temperature near zero displacement in the case of sinusoidal unidirectional excitation when the input friction heating is large, and this weakness will be enlarged if the slider diameter increases. In another hand, this model is considered to have good performance under earthquake excitation because earthquakes are excitations with random orbits, which means that the input friction heating will not be extremely large on some certain area (in the case of sinusoidal unidirectional excitation, the friction heating input near zero displacement is extremely large).

In addition, a simplified model based on the precise model was introduced, which also shows high accuracy in the calculation of force-deflection characteristics under various conditions. In addition, the calculation speed of the simplified model is much higher than that of the precise model. However, the weakness of this model is also obvious. Since only one analytical monitor point at the centre is considered, force jumps will occur when the horizontal displacement of the DCFPB is half of the slider diameter. Moreover, due to the force jump, the calculation of force-deflection characteristics will have lower accuracy when the oscillation amplitude is larger than the slider diameter. Based on these results, this simplified model can be applied instead of a precise model when the maximum displacement is less than half of the slider diameter. Additionally, with the displacement approaches the slider diameter, a force jump can be observed, but the influence is not considered to be significant. However, if the maximum displacement exceeds the slider diameter, the simplified model is not recommended.

A constant model with reference friction coefficient μ0 is also introduced for each specimen size, and the determination method of $\mu_0$ is introduced. The main idea of this model is to obtain a constant friction coefficient $\mu_c$ (based on $\mu_0$) that can make the simulation result acceptable under most seismic loading conditions. A comparison of the accuracy of the hysteresis curves and force-deflection characteristics of the constant model with the results of the precise model shows that the constant model gives acceptable fitness under most situations except extremely low friction heating input, such as wind load, and extremely high friction heating input situations, such as large number of cycles. Therefore, a constant friction coefficient can be used to simulate the behaviour of FPBs under sinusoidal unidirectional excitation without significant differences if a suitable value is chosen.

## 5. Acknowledgments

The assistance of Dr. Cameron J. Black, Dr. Ian D. Aiken and Professor Gianmario Benzoni during the experiment at the University of California, San Diego, is highly appreciated.



 

## 5. Reference

[1] V. Quaglini, P. Dubini and C. Poggi, 2012. Experimental assessment of sliding materials for seismic isolation systems, Bull Earthquake Eng 10, 717–740.

[2] G. Lomiento, N. Bonessio and G. Benzoni, 2013. Friction Model for Sliding Bearings under Seismic Excitation, Journal of Earthquake Engineering, 17, 1162–1191.

[3] V. Quaglini, M. Bocciarelli, E. Gandelli and P. Dubini, 2014. Numerical Assessment of Frictional Heating in Sliding Bearings for Seismic Isolation, Journal of Earthquake Engineering, 18, 1198-1216.

[4] M. Kumar, AS. Whittaker, and MC. Constantinou, 2015. Characterizing friction in sliding isolation bearings, Earthquake Engng Struct. Dyn, 44, 1409–1425

[5] V. Bianco, D. Bernarddini, F. Mollaioli and G. Monti, 2018. Modeling of the temperature rises in multiple friction pendulum bearings by means of thermomechanical rheological elements, Archives of Civil and Mechanical Engineering, 19, 171–185

[6] G. Benzoni and F. Seible, 1998. Design of the Caltrans Seismic Response Modification Device (SRMD) test facility (IWGFR--96), International Atomic Energy Agency (IAEA), International Working Group on Fast Reactors, Vienna (Austria), 325 p, p. 101-115

[7] American Society of Civil Engineers (ASCE), 2016. Minimum Design Loads and Associated Criteria for Buildings and Other Structures, ASCE/SEI 7-16, Reston, VA.

[8] K. Nishimoto, H. Nakamura, H. Hasegawa, and N. Wakita, 2016. Bearing Stress and Velocity Dependency of Spherical Sliding Bearing through Full-scale tests, Paper No. 21223, Summaries of Technical Papers of Annual Meeting, Architectural Institute of Japan, 24-26 August, 2016, Fukuoka, Japan. (in Japanese).

[9] H. Nakamura, K. Nishimoto, H. Hasegawa, and H. Nakamura, 2015. Predictive Method of a Temperature Rise and the Friction Coefficient of Spherical Sliding Bearing (Part 3), Paper No. 21232, Summaries of Technical Papers of Annual Meeting, Architectural Institute of Japan, 4-6 September, 2015, Kanto, Japan. (in Japanese).

[10] S. Yamazaki, K. Nishimoto and A. Watanabe, 2019. Experimental and Analytical Study of Spherical Sliding Bearing for Long Period Ground Motion, in press, Summaries of Technical Papers of Annual Meeting, Architectural Institute of Japan, 3-6 September, 2019, Hokuriku, Japan. (in Japanese).

[11] MC. Constantinou, AS. Whittaker, Y. Kalpakidis, DM. Fenz, GP. Warn, 2007. Performance of seismic isolation hardware under service and seismic loading. Multidisciplinary Center for Earthquake Engineering Research, Report No. MCEER-07-0012, Buffalo, NY.

[12] Japan Society of Mechanical Engineers (JSME), 2009. Heat Transfer, 5th edition, JSME Data Books, Tokyo, JP, 284-285.



 